Int. J. Adv. Eng. Pure Sci. 2023, 35(1): 1-9
DOI: 10.7240/jeps.1062072

RESEARCH ARTICLE / ARAŞTIRMA MAKALESİ

Construction of $CaTiO_3$/g-C_3N_4 Heterostructure for Boosting Photodegradation of Indigo Carmine under Visible Light Illumination

Özlem TUNA[1]

[1]*Department of Chemical Engineering, Faculty of Engineering, Yalova University, 77100 Yalova, Türkiye*

Abstract
Graphitic carbon nitride (CN) modified $CaTiO_3$ (CTO) heterostructures were fabricated and utilized in photocatalytically indigo carmine (IC) decomposition. The CTO/CN(III) heterostructure exhibited the best photocatalytic performance for IC degradation under visible light irradiation. For the optimal sample, the apparent rate constants of the reaction were 1.69 and 10.50 times that of CN and CTO, respectively. This could be due to the satisfactory separation of photoinduced species in an easy way. The photocatalyst dosage increased the removal efficiency, while the initial dye concentration negatively affected the IC degradation rate. Under acidic condition, the catalyst showed superior degradation rate. Moreover, the superoxide radicals ($\bullet O_2^-$) was the most effective carrier for IC photodegradation and depending on the results of the trapping agent experiments, the possible photocatalytic reaction mechanism of CTO/CN(III) sample was proposed. In addition, the composite achieved considerable performance in ions-included water bodies, namely tap water and drinking water. This study provides a promising and stable photocatalyst as a graphitic carbon nitride modified with calcium-based perovskite for dye removal.

Keywords: $CaTiO_3$, graphitic carbon nitride, indigo carmine, photocatalyst

I.INTRODUCTION

Dye components have been detected in different water environments obtained from various industries especially textile and paint industries. Indigo carmine (IC), one of the oldest dyes, has been applicated in foods, drugs, clothes. The occurrence of IC in water body has potential negative effects on human and aquatic organisms [1]. The removal of the organic dye in the industrial wastewater has become an important research subject in the field of environmental management. In this case, various attempts have been applied as physicochemical and biological methods, namely coagulation–flocculation, electrocoagulation, adsorption, ion exchange irradiation, ultrasound, membrane filtration, ozonation, electrochemical destruction [2,3]. Apart from these attempts, degrading the organic pollutant to CO_2 and H_2O by photo-induced process is one of the most promising way due to its the high efficiency and safety properties [1]. In this field, perovskites have been widely concerned as functional materials due to their unique features, namely excellent strong oxidation ability, durable stability, high compositional and structural flexibility [4]. Perovskites have been generally presented with the general formula ABO_3. In this crystal structure, the A site is occupied by the larger cation, while the B site is occupied by the smaller cation [5].

Calcium titanate ($CaTiO_3$), n-type semiconductor, is one of the most important perovskite material that shows satisfactory photoluminescent, and excellent dielectric polarization properties, resulting that it can be successfully used in optical and electrical applications [6]. However, the titanate-based perovskite has drawbacks, such as lack of active sites, wide band gap energy (3.4 eV), and weak charge carrier extraction, resulting in low photocatalytic degradation performance [7]. To overcome the drawbacks, research efforts have been dedicated to modulating the energy level of the perovskite that provides bandgap tuning toward the visible range and the efficient separation of electron-hole pairs. For that, recent approach is to construct heterojunction photocatalysts by incorporate $CaTiO_3$ perovskite with different structures.

Graphitic carbon nitride (g-C_3N_4) has been deemed as an efficient candidate to improve the activity of $CaTiO_3$ in photocatalysis field due to its excellent thermal and chemical stability with unique optoelectronic properties [8]. The polymeric carbon nitride is constructed by the building blocks of triazine or tri-s-triazine (heptazine) rings bridged with the conjugated N atoms to the 2D layer structure [9]. The free electrons of N atoms can provide activating under visible light illumination. However, the abre graphitic graphitic carbon nitride depicts low photocatalytic activity due to its high recombination rate of the photo-induced charge carriers [10]. In this point, the couple g-C_3N_4 with perovskites has been important to decrease the recombination rate of the electron-holes of the pristine g-C_3N_4. The incorporation of g-C_3N_4 with perovskites enable the band structure of the heterojunction to be well positioned, resulting in excellent visible light absorption and superior charge separation ability [11].

Corresponding Author: ÖZLEM TUNA, e-posta: ozlemmtuna@gmail.com

Submitted: 23.01.2022, **Revised:** 02.03.2023, **Accepted:** 08.01.2023

In this case of perovskite, $LaFeO_3$ [12-15], $LaMnO_3$ [16], $LaNiO_3$ [17,18] and $SrTiO_3$ [19-21] have been widely used to design the heterojunction photocatalyst. Besides these, $CaTiO_3$ has been utilized in the improvement of the graphitic carbon nitride of photocatalytic efficiency. Pan et al. [22] synthesized $CaTiO_3/g\text{-}C_3N_4$ by performing hydrothermal followed by deposition method. The interaction increased the H_2 production rate of the bare perovskite due to sufficient the separation rate of the photogenerated charge species. In other study, the photocatalytic activity of $CaTiO_3/g\text{-}C_3N_4$ was examined in the degradation of crystal violet (CV) and malachite green (MG) under sunlight irradiation [23]. Kumar and co-workers [24] depicted that graphitic carbon nitride nanosheets (CTCN) provided good excitation dissociation at interface for the photoinduced electrons-holes pairs in $CaTiO_3$/ CTCN photocatalyst. They also obtained efficient organic molecule degradation rates by performing it under sunlight irradiation. Although the relevant studies showed that $g\text{-}C_3N_4$-incorporated with $CaTiO_3$ could be successively used in photocatalytic process driven by sunlight irradiation, to our knowledge, no study has examined the photocatalytic efficiency of $CaTiO_3/g\text{-}C_3N_4$ sample under visible light illumination. Therefore, in this study $CaTiO_3$ was interacted with $g\text{-}C_3N_4$ to obtain satisfactory IC degradation under visible light irradiation.

Herein, we report the synthesis of $CaTiO_3/g\text{-}C_3N_4$ photocatalysts by hydrothermal method and their utilization in photocatalytic degradation of indigo carmine dye at first time. The effect of graphitic carbon nitride amount on the catalytic reaction was examined under visible as well as UV-A light irradiations, as well as dark conditions. By using optimum photocatalyst, the decomposition efficiency was evaluated under different catalyst dosage and initial dye concentration. The effects of different factors (pH, active substance, water body, and reusability) on the removal efficiency were examined, and subsequently, photocatalytic mechanisms for IC degradation were proposed.

II. MATERIALS AND METHODS

2.1. Chemicals

$CaCl_2{\bullet}2H_2O$, $FeCl_3{\bullet}9H_2O$ (99%) and CH_4N_2O were supplied from Merck. Melamine was obtained from Iso Lab. The other chemicals as IPA (70%), EDTA-2Na (≥ 98.5%), BQ (≥98%), NaOH and HCl (37%) were obtained from Merck and Isolab. Indigo carmine (IC), common synthetic dye, was performed as model pharmaceutical pollutant. All chemicals were applied without purification and distilled water was utilized for all experiments.

2.2. Preparation of photocatalysts

Sole graphitic carbon nitride ($g\text{-}C_3N_4$) material was synthesized by heating melamine to 550 ºC in a semi-closed crucible with a heating rate of 3 ºC min^{-1} under air condition and the temperature was maintained at stable for 3 h. After cooling to room temperature, the yellowish $g\text{-}C_3N_4$ powder was obtained [12]. The final sample was labeled as CN. On the other hand, pristine $CaTiO_3$ particles (CTO) were fabricated by performing hydrothermal method. Primarily, 1.109 g $CaCl_2.\ 2H_2O$ was dissolved in basic aqueous solution, and simultaneously 3.404 g $Ti(C_4H_9O)_4$ was dissolved in 10 mL ethanol. Next step, the calcium salt solution was added drop by drop into the titanium-included solution under rigorous stirring for 2h. Thereafter, the solution was placed in autoclave and treated at 180 °C for 18 h. Finally, the precipitation was dried at 60 °C for overnight followed by calcination at 600 °C for 3 h [25]. The final photocatalyst was named as CTO.

CTO-incorporated with CN heterostructures were produced by performing hydrothermal method. In this method, the certain CTO amount was distributed in distilled water (30 mL), then the specific amount of CN was added into the dispersion. After that, the precursor solution was homogenized in a ultrasonic bath and it was further mixed under vigorously stirring for 3 h at ambient temperature. Then, the mixture was treated at 200 ºC in for 18 h in an autoclave. The resultant sample was washed and dried. Finally, the as-fabricated powder was obtained. According to the synthesis method, three CTO/CN photocatalysts were fabricated with various carbon nitride amount. The weight ratio of CTO:CN was determined as 1:0.25, 1:0.50, and 1:1, as well as the heterostructures were named as CTO/CN(I), CTO/CN(II), and CTO/CN (III), respectively.

2.1. Characterization

The crystalline properties of the as-obtained heterostructured photocatalysts were identified by performing X-ray powder diffraction (XRD) analysis (Panalytical X'Pert PRO Model). The morphology of the samples was monitored using a field-emission scan electron microscopy (SEM-EDAX: Bruker). In order to examine the optical features of the samples, UV–vis diffuse reflectance spectra (DRS) analysis was performed.

2.4. Photocatalytic Experimental Studies

Photocatalytic degradation of indigo carmine was studied in a glass reactor placed into a square cabinet including two visible lamps (Osram 150 W, λ: 400–800 nm). During the reaction, a fan-cooling system was utilized to ensure the temperature of the reaction solution at ambient level. The reaction solution was stirred magnetically for 30 min to achieve adsorption-desorption equilibrium in dark. During the photocatalytic experiment, aliquots (3 mL) were taken at time intervals from 30 to 120 min and filtered using a syringe filter. Then, the concentration of the residual IC was evaluated by the absorbance at 552 nm [26].

To observe the effect of catalyst dosage on the removal efficiency, the photocatalytic experiments were performed under various catalyst dosage (0.1, 02, and 0.3 g/L). Also, the role of the initial dye concentration was evaluated by considering the performance in the presence of 5, 10 and 15 mg/L IC. Furthermore, the effect of solution pH was determined by performing the photocatalytic test under alkaline and acidic environments. Scavenger tests were also conducted to identify the main radical oxidative species (ROS) in visible-light-assisted IC degradation by using h^+, •OH, and $•O_2^-$ trapping agents (EDTA-2Na, IPA and BQ, respectively). Moreover, the reaction was carried out in case of drinking water and tap water media. Bu using the water sources, IC solutions with the concentration of 10 mg/L were prepared. In addition, the chemical stability of CTO/CN sample was investigated by reusing five times in the catalytic system. After each cycle, the fresh dye with desired concentration was spiked into the solution for further run. In this study, all experiments were performed in triplicate and average results were reported.

The degradation rate of IC was determined by following Equation (1):

$$\text{Removal Efficiency } \% = (C_0\text{-}C)/C_0 \times 100\% \quad (1)$$

where C_0 and C are the initial and final concentrations (mg/L) at 0 and t min of irradiation time, respectively. Also, the reaction kinetic properties were illustrated by pseudo-first-order kinetics based on the following Equation (2).

$$\ln(C_{in}/C_{out}) = kt \quad (2)$$

where C_{in} and C_{out} are the starting and final concentrations of IC in the reaction process, and the slope k (min^{-1}) and t (min) are the apparent rate constant and reaction time, respectively.

III. RESULTS AND DISCUSSION

3.1. Characterization

The phase structures of the pristine g-C_3N_4, $CaTiO_3$ and the as-fabricated heterostructure ($CaTiO_3$/g-C_3N_4) were thoroughly investigated using XRD. Figure 1 illustrates the XRD patterns of the samples. The dominant diffraction peaks (2θ) represented $CaTiO_3$ crystal plans of (111), (121), (002), (220), (202), (212), (042) (004), and (242), respectively (ICDS 06-2149) [27,28]. Furthermore, the diffraction peak appeared at 27.5º was attributed to the presence of g-C_3N_4 [23]. In case of CTO/CN, besides the main peaks of CTO sample, the peak corresponding to the crystal phase of CN was observed in the composite. The results showed that CTO/CN was successfully synthesized by performing the hydrothermal method in this study.

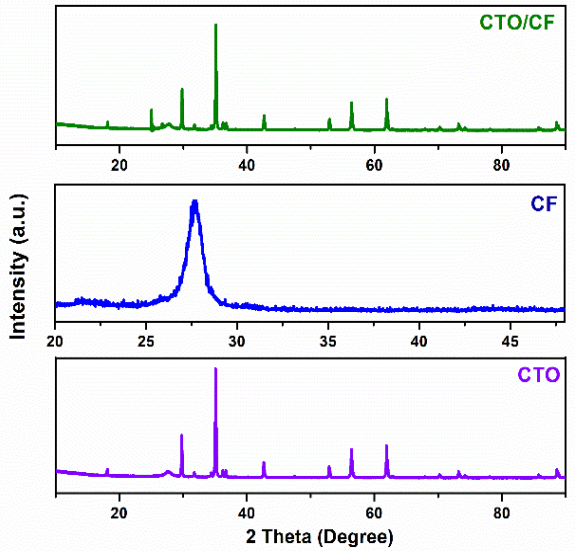

Figure 1. XRD spectrums of CTO, CN and CTO/CN(III) samples

SEM was employed to identify the micromorphology and composition of the as-prepared materials. The SEM photos of the samples are presented in Figure 2. The formation of CTO particles in cubic morphology was observed in this figure. Moreover, irregular rod shapes were depicted on the material indicating the occurrence of particle agglomeration during the preparation section. In terms of CN, the image showed layer structure with a relatively smooth and flat surface. In addition, it could be obviously observed that the dispersity of CTO particles formed on the surface of g-CN sheets, which was assigned to the formation of CTO/CN composite.

UV–vis and diffuse reflectance spectroscopy was conducted to determine the light absorption properties of the perovskite and the carbon-based material (Figure 3). CN showed wider the wavelength region of the irradiated light than that of CTO. It was suggested that the incorporation of graphitic carbon nitride into $CaTiO_3$ could effectively extend the light absorption capacity. The indication was supported with the efficiency of CTO/CN in the photocatalytically IC degr images of CTO, CN and CTO/CN(III) samples.

3.2.Primarily photocatalytic dye degradation

To investigate the photocatalytic efficiency of pristine (CN), sole CaTiO3, and CaTiO3-incorparated with CN samples (CTO/CN(I), CTO/CN(II), and CTO/CN (III)), the indigo carmine degradation was performed under visible light and UV-A light illumination, as well as dark conditions (Figure 4). Observing the dark adsorption performances of the catalysts, the removal efficiencies were calculated as 10.17%, and 39.39% for bare CN and CaTiO3, respectively. The dye adsorption ability enhanced with increasing carbon-based constituent: CTO/CN(I), CTO/CN(II) and

CTO/CN(III) showed 47.01%, 48.18% and 49.56% indigo carmine removal (Figure 4a).

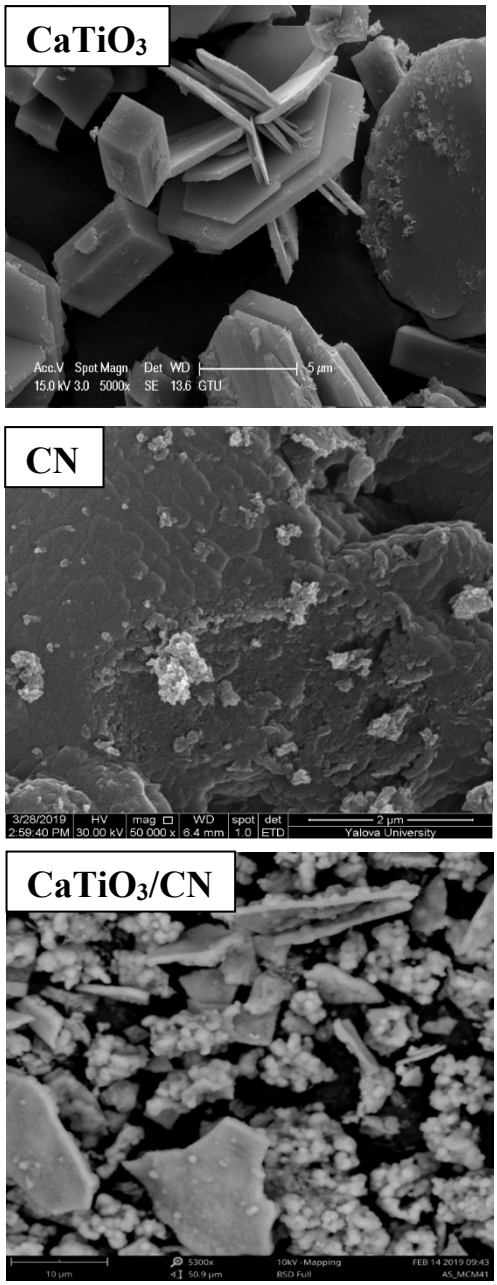

Figure 2. SEM images of CTO, CN and CTO/CN(III) samples

The results indicated that electrostatic attraction and hydrogen bonding between the functional groups of the dye components (C=O, N-H and SO_3) and the active species of the CN facilitated the indigo carmine adsorption on the samples [29]. In terms of UV-A light-driven removal, the incorporation CN into CTO improved the reaction rate; the IC removal values of CTO/CN(I), CTO/CN(II) and CTO/CN(III) were found as 77.51%, 95.30% and 97.04%, respectively (Figure 4b). Similar behavior was observed under visible light illumination; CTO/CN(III) depicted significant the photodegradation efficiency (76.38%) (Figure 4c). Furthermore, all removal rates were higher than that of bare CN and CTO. This could be due to the synergetic effect of the composite material that improved adsorption ability. Thus, it could be concluded that the photocatalytic IC decomposition property was boosted the contributions of graphitic carbon nitride, which was assigned to enhanced visible light absorption ability. In addition, the degradation rate constants (k, min^{-1}) were found to be 0.007, 0.0084 and 0. 0108 min^{-1} for the CTO/CN(I), CTO/CN(II) and CTO/CN(III) photocatalysts, respectively. The maximum rate constant was obtained by utilizing CTO/CN(III) and therefore, the photocatalyst were used in subsequent experiments.

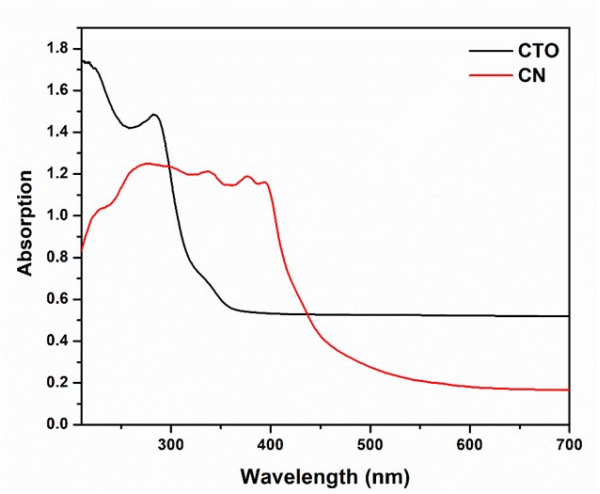

Figure 3. UV–Vis DRS spectra of CTO and CN

3.3.Effect of catalyst dosage

The experiment results of the effect of catalyst dosage on the degradation efficiency are plotted in Figure 5a. It was observed that with increasing catalyst dose from 0.10 to 0.30 g/L, the efficiency of dye degradation was increased from 68.34% to 99.02%. This increment was also reflected in the reaction coefficient values; the k constant was calculated as 0.0088, 0.0108 and 0.0349 min^{-1} for 0.10, 0.20 and 0.30 g/L, respectively. The increase trend can be due to the enhancement in the surface area or active sites for reaction of the indigo carmine molecules.

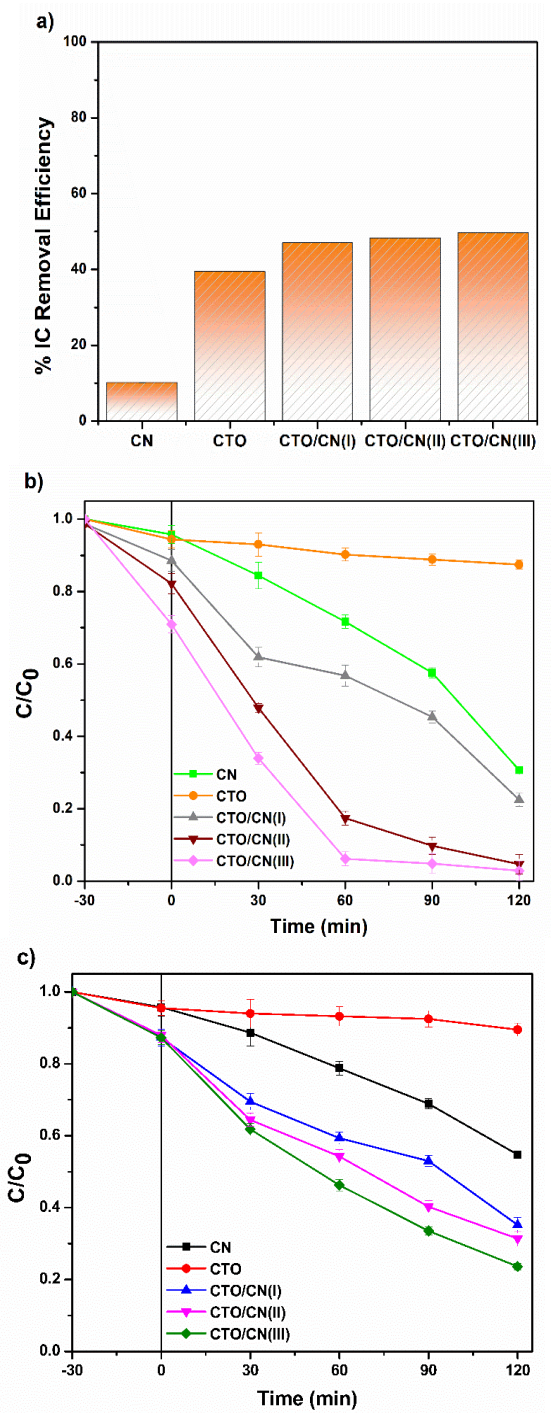

Figure 4. (a) Photocatalytic indigo carmine degradation studies in dark environment, **(b)** under UV-A light irradiation and **(c)** under visible light irradiation (0.2 g/L of catalyst dosage and 10 mg/L of IC concentration)

3.4. Effect of initical dye concentration

Figure 5b depicts the plot of degradation vs time with respect to different initial dye concentrations (5-15 mg/L). It showed the highest efficiency (86.41%) at mere low initial concentration of the dye (5 mg/L), which was attributed to the adsorption of dye molecules onto the catalyst surface and immediately dye degradation. As the initial solution concentration increased, the degradation efficiency reduced. In case of high IC amount, more dye molecules were adsorbed onto the surface of CTO/CN; however, the adsorbed dye molecules were not able to immediately degrade. Since, the light intensity on the photocatalyst surface decreased, resulting that the path length of the photons entering the solution was increased due to more colored reaction mixture. Hence, the production of radicals which were effective on the IC decomposition was limited. In addition, the reaction rate constants were calculated as 0.0139, 0.0108 and 0.0073 min^{-1} in the presence of 5, 10 and 15 mg/L dye concentration, respectively.

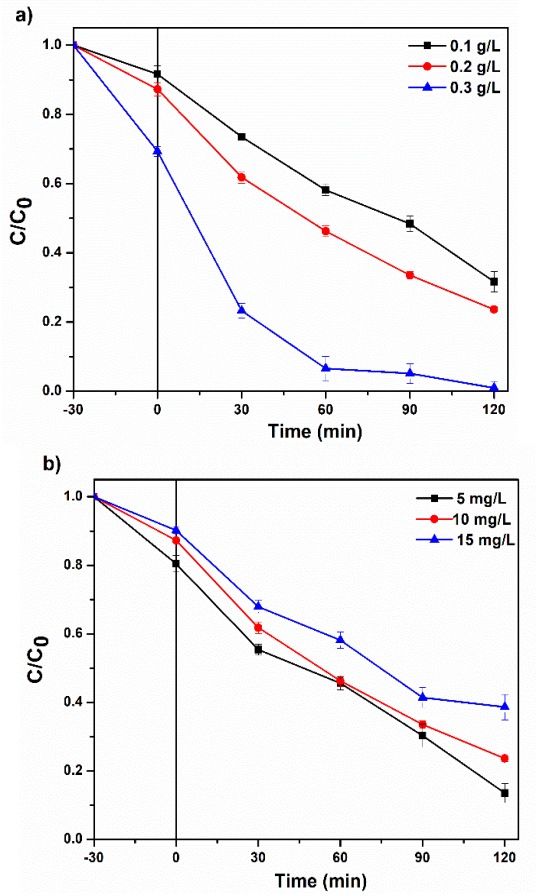

Figure 5. (a) The effect of catalyst dosage and **(b)** the effect of initial dye concentration on dye removal in the presence of CTO/CN(III)

3.5. Effect of pH

In terms of dye degradation in wastewater, pH value is an essential factor, since the property significantly affects the adsorption of the organic molecule on catalyst surface, which is first step of the degradation. Figure 6a depicts the photocatalytic performances at different pH values. The maximum removal efficiency (90.81%) was observed under acidic condition (pH 3). When the solution pH value changed from 6 to 10, the decomposition efficiency declined from 76.38% to 44.44%. On the other hand, the activity changes driven by pH value of reaction environment could be due to

the charge features of active species and pKa value of IC dye at various pH values. IC molecule possesses pKa value of 12.6, and therefore it predominantly exists as anionic form, also it is negatively charged in a wide pH range. Thus, it was stated that the sorption could be improved by enhanced electrostatic attraction between negatively charged dye component and positively charged photocatalyst at pH 3. Furthermore, at pH values around 10, the rate of dye removal limited due to a gradual loss of the positive charges on the adsorbent surface and partly due to the competition between the medium OH– and the anionic dye to interact with the adsorbent surface. The results were indicated that the performance of IC decomposition on CTO/CN (III) was unfavorable under alkaline condition. Similar phenomenon was observed by other researchers [30,31].

3.6. Effect of scavengers

To determine the mechanism of the photocatalytic indigo carmine degradation on CTO/CN (III), free radical capture experimental studies were carried out. IPA, EDTA-2Na and BQ, were selected as scavengers for •OH, h^+ and $\bullet O_2^-$, respectively. As observed in Figure 6b, the catalytic performance was significantly limited, when the trapping agent for superoxide radical was added into the reaction solution. That is, the activity decreased from 76.38.% (no scavenger: control experiment) to 18.13%. The observation showed that $\bullet O_2^-$, could be considered as the most effective reactive oxygen species in the visible light driven-indigo carmine removal process. In terms of EDTA-2Na and IPA, the decomposition efficiency partly decreased to 72.14% and 71.13%, respectively, indicating that h^+ and •OH had minor contributions on the degradation.

The potential mechanism for the decomposition reaction of indigo carmine over CTO/CN (III) was presented in Figure 7. Firstly, light photons were observed on the heterostructure. The photogenerated electrons accumulated on the CB of CTO reduced O_2 molecules adsorbed on the composite catalyst surface to superoxide radicals. Then, indigo carmine was mainly decomposed to smaller dye molecules by the reactive groups. Besides, the photo-induced holes on the VB of CN and •OH radicals was obtained via serial reactions facilitated the oxidization of IC. Finally, the organic molecule further degraded into CO_2 and H_2O

3.7. Effect of water bodies

To further examine the availability of CTO/CN (III) as a photocatalyst for wastewater treatment, the dye degradation was assessed in different water media namely, distilled, drinking water and tap water. As observed in Figure 6c, the removal performances were found as 76.38%, 73.98% and 71.3% in case of distilled water, tap water, and drinking water, respectively; stating that the performance slightly affected from the type of aqueous phase.

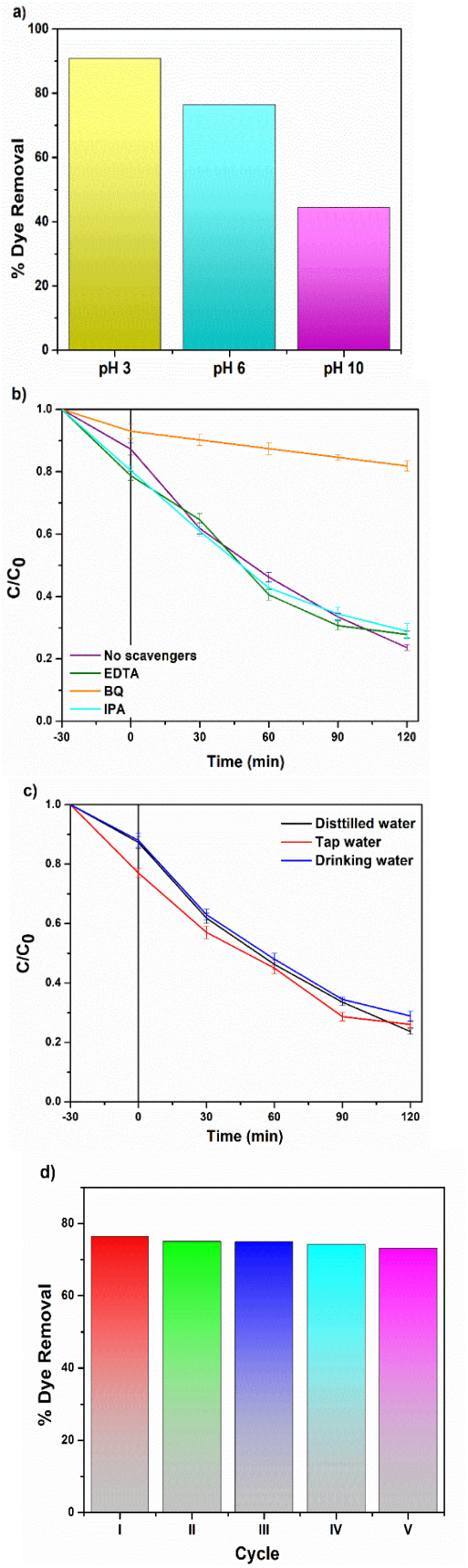

Figure 6. (a) The effect of solution pH, **(b)** scavengers, **(c)** water medium and **(d)** reusability of CTO/CN(III) on dye removal

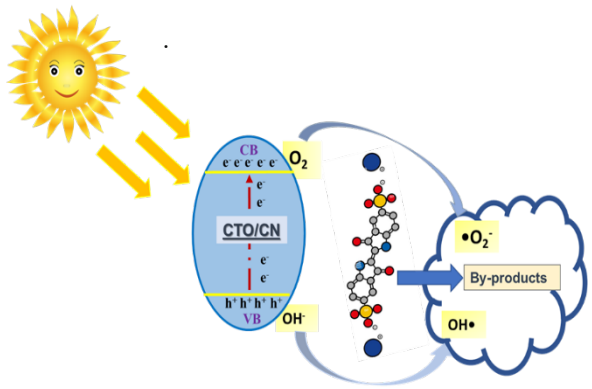

Figure 7. Schematically possible degradation mechanism

The change could depend on the many parameters, especially the pH of the reaction environment, charged ions, and organic contaminants. The most effective inhibition resulted from SO_4^{2-} and Cl^-, which were more dominant species in tap and drinking water bodies. Since the competitive adsorption between anions and IC molecules on the photocatalyst surface occurred. Therefore, it could be indicated that the dye removal rate was limited by the competitive adsorption driven by anions.

3.8. Reusabiility

For practical and full-scale industrial application, the most important consideration is to investigate reusability of photocatalysts. In view of this, five successive photocatalytic experiments were performed under visible light irradiation to examine the stability of CTO/CN (III) sample. As presented in Figure 6d, only 4.29% reduction in IC degradation rate was observed after fifth cycle. It could be concluded that CTO/CN heterostructure provided excellent stable photocatalytic efficiency for indigo carmine degradation.

IV. CONCLUSION

In summary, $CaTiO_3$/g-C_3N_4 photocatalysts were effectively produced by a simple hydrothermal method, in which graphitic carbon nitride particles were anchored with the perovskite. The as-prepared CTO/CN composites exhibited good photocatalytic activity for the degradation of IC under visible and UV-A light irradiation. The weight ratio CTO:CN of 1:1 (CTO/CN(III)) performed highest photocatalytic degradation efficiency of 97.09% and 76.38% in the presence of 120 min under UV-A and visible light irradiation, respectively. The characterization revealed that the reason for improving photocatalytic performance was to enhance the incident light trapping ability and promote separation of photo-induced charges. With increasing photocatalyst dosage, the catalytic performance improved, resulting increase active sites. However, the efficiency decreased, and this might be attributed to overlapping or aggregation of adsorption sites. The dye degradation was significantly driven by super oxide radicals. Interestingly, CTO/CN(III) showed good activity under tap water and drinking water. In addition, the catalyst exhibited high performance even if after five-cycle experiment, stating stable photocatalyst for dye removal. This study provides a new perspective for the application of $CaTiO_3$-based carbon nitride-based composites in photocatalytic degradation of organic pollutants.

ACKNOWLEDGMENT

This study was supported by Yalova University (project no. 2022/AP/0003).

REFERENCES

[1] Ferdous, M., Khander, S., Sarker, F., Islam, A. (2020). Current treatment technologies and mechanisms for removal of indigo carmine dyes from wastewater : A review. *J. Mol. Liq*., 318, 114061.

[2] Flox, C., Ammar, S., Arias, C., Brillas, E. (2006). Electro-Fenton and photoelectro-Fenton degradation of indigo carmine in acidic aqueous medium, *Appl. Catal,*.67, 93–104.

[3] Bafana, A., Devi, S., Chakrabarti, T. (2011). Azo dyes : past , present and the future. *Environ. Rev.*, 370, 350–370.

[4] Lin, N., Gong, R., Wang, Y., Zhang, X. (2022). Critical review of perovskite-based materials in advanced oxidation system for wastewater treatment : Design , applications and mechanisms, *J. Hazard. Mater*. 424, 127637.

[5] Kanbere, P., Chen, Z. (2014). A Review on Visible Light Active Perovskite-Based Photocatalysts, *Molecules*, 19, 19995-20022.

[6] Kov, T. (2021). Nano and micro-forms of calcium titanate : Synthesis , properties and application, *Open Ceramics*, 8, 100177.

[7] Passi, M., Pal, B. (2021). A review on $CaTiO_3$ photocatalyst : Activity enhancement methods and photocatalytic applications. *Powder Technol.*, 388, 274–304.

[8] Nasir, M.S., Yang, G, Ayub, I., Wang, S., Wang, L., Wang, X., Yan, W., Peng, S., Ramakarisha, S. (2019). Recent development in graphitic carbon nitride based photocatalysis for hydrogen generation. Appl. Catal. B Environ. 257:117855.

[9] Ong, W.J., Tan, L.L., Ng, Y.H., Yong, S.T., Chai, S.P. (2016). Graphitic carbon nitride (g-C3N4)- based photocatalysts for artificial photosynthesis and environmental remediation: are we astep closer to achieving sustainability?. *Chem. Rev.* 116:7159–7329.

[10] Zhao, Z., Sun, Y., & Dong, F. (2015). Graphitic carbon nitride based nanocomposites: a review. *Nanoscale*. 7(1), 15-37.

[11] Khan, M. S., Zhang, F., Osada, M., Mao, S. S., & Shen, S. (2020). Graphitic carbon nitride-based low-dimensional heterostructures for photocatalytic applications. *Solar RRL* 4(8), 1900435.

[12] Acharya, S., Mansingh, S., Parida, KM. (2017). The enhanced photocatalytic activity of g-C3N4-LaFeO3 for the water reduction reaction through a mediator free Z-scheme mechanism. *Inorg.Chem. Front.* 4:1022–1032.

[13] Ye, Y., Yang ,H., Wang, X., Feng, W. (2018). Photocatalytic, Fenton and photo-Fenton degradation of RhB over Z-scheme g-C3N4/LaFeO3 heterojunction photocatalysts. *Mater. Sci. Semicond. Process*. 82:14–24.

[14] Ismael, M., Wu, Y. (2019). A facile synthesis method for fabrication of LaFeO3/g-C3N4 nanocomposite as efficient visible-light-driven photocatalyst for photodegradation of RhB and 4-CP. *New J. Chem*, 13783–13793.

[15] Zhang, J., Zhu, Z., Jiang, J., Li, H. (2020). Fabrication of a novel AgI/LaFeO3/g-C3N4 dual Zscheme photocatalyst with enhanced photocatalytic performance. *Mater. Lett.* 262:127029.

[16] Luo, J., Chen, J., Guo, R., Qiu, Y., Li, W., Zhou, X., Ning, X. (2019). Rational construction of direct Z-scheme LaMnO3/g-C3N4 hybrid for improved visible-light photocatalytic tetracycline degradation. *Sep. Purif. Technol.* 211:882–894.

[17] Zhou, X., Chen, Y., Li, C., Zhang, L., Zhang, X., Ning, X,. Zhan, L. (2019). Construction of LaNiO3 nanoparticles modi fi ed g-C3N4 nanosheets for enhancing visible light photocatalytic activity towards tetracycline degradation. *Sep. Purif. Technol.* 211:179–188.

[18] Ye, C., Wang, R., Wang, H., Jiang, F. (2020). The high photocatalytic efficiency and stability of LaNiO3/g-C3N4 heterojunction nanocomposites for photocatalytic water splitting to hydrogen. *BMC Chem.* 14:1–13.

[19] Konstas, P., Konstantinuo, I., Petrakis, D., Albanis, T. (2018). Synthesis, characterization of gC3N4/SrTiO3 heterojunctions and photocatalytic activity for organic pollutants degradation. *Catalys.* 8(11):554.

[20] Luo, Y., Deng, B., Pu, Y., Liu, A., Wang, J., Ma, K., Gao, F. (2019). Interfacial coupling effects in g-C3N4/SrTiO3 nanocomposites with enhanced H2 evolution under visible light irradiation. *Appl. Catal. B Environ*. 247:1–9.

[21] Tan, C.E., Lee J.T., Su, E.C.,Wey, M.Y. (2020). Facile approach for Z-scheme type Pt/g-C3N4/SrTiO3 heterojunction semiconductor synthesis via low-temperature process for simultaneous dyes degradation

[22] Pan, J., Jiang, Z., Feng, S., Zhao, C., Dong, Z., Wang, B., Wang, J., Song, C., Zheng, Y. (2018). The enhanced photocatalytic hydrogen production. *Int. J. Hydrogen Energy*. 43:19019–19028.

[23] Chen, X., He, X., Yang, X., Wu, Z., Li, Y. (2020). Construction of novel 2D/1D g-C3N4/CaTiO3 heterojunction with face-to-face contact for boosting photodegradation of triphenylmethane dyes under simulated sunlight. *J. Taiwan. Inst. Chem. Eng.* 107:98–109.

[24] Kumar, A., Schuerings, C., Kumar, S., Kumar, A., Krishnan, V. (2018). Perovskite-structured CaTiO3 coupled with g-C3N4 as a heterojunction photocatalyst for organic pollutant degradation. *Beilstein. J. Nanotechnol.* 9:671–685.

[25] Simsek, E. B. (2022). Construction of CaTiO3 nanosheets with boron nitride quantum dots as effective photogenerated hole extractor for boosting photocatalytic performance under simulated sunlight. *Ceramics* International.

[26] Balta, Z. Simsek, E. B. (2022). Understanding the structural and photocatalytic effects of incorporation of hexagonal boron nitride whiskers into ferrite type perovskites (BiFeO3, MnFeO3) for effective removal of pharmaceuticals from real wastewater. *J. Alloys. Compd,* 898, 162897.

[27] Han, J., liu, Y., Dai, F., Zhao, R., Wang, L. (2018). Fabrication of CdSe / $CaTiO_3$ nanocomposties in aqueous solution for improved photocatalytic hydrogen production. *Appl. Surf. Sci.*, 459, 520–526.

[28] Holliday, S., Stanishevsky, A. (2004). Crystallization of $CaTiO_3$ by sol – gel synthesis and rapid thermal processing. *Surf. Coat. Technol.*, 189, 741–744.

[29] Khadhri, N., El, M., Saad, k., Moussaoui, Y. (2019). Batch and continuous column adsorption of indigo carmine onto activated carbon derived from date palm petiole. *J. Environ. Chem. Eng.* 7, 102775.

[30] Kas, H. (2005). Aminofunctionalized acrylamide – maleic acid hydrogels :

Adsorption of indigo carmine. Colloids Surf. A Physicochem. Eng., 266, 44–50.

[31] Donneys-victoria, D., Machuca-martínez, F. (2020). Indigo carmine and chloride ions removal by electrocoagulation . Simultaneous production of brucite and layered double hydroxides. J. Water Process Eng., 33, 101106.